J. Cent. South Univ. (2022) 29: 3884−3895
DOI: https://doi.org/10.1007/s11771-022-5199-y

Springer

Mechanical activation of natural chalcopyrite for improving heterogeneous Fenton degradation of tetracycline

WANG Chong-qing(王重庆), YANG Jia-peng(杨嘉鹏), HUANG Rong(黄荣), CAO Yi-jun(曹亦俊)*

School of Chemical Engineering, Zhengzhou University, Zhengzhou 450001, China

Abstract: Natural minerals receive growing attention as inexpensive, green, and efficient catalysts for degradation of organic pollutants. Mechanical activation of natural chalcopyrite was conducted for improving the catalytic performance. Tetracycline degradation was evaluated in the presence of hydrogen peroxide and mechanically activated chalcopyrite. Tetracycline degradation at 100 min is 55.52% (Chp10), 68.97% (Chp30), 77.79% (Chp60), and 86.43% (Chp120), respectively, and the rate constant of pseudo-first-order kinetics is 0.0079, 0.0109, 0.0137 and 0.0192 min^{-1}, respectively. Chalcopyrite samples were examined by multiple characterizations. Mechanical activation of natural chalcopyrite induces the decline of particle size and slight increase of surface area, smaller grain size, lattice strain, and partial sulfur oxidation. The relationship between catalytic activity and property change manifests that the improved catalytic ability is mainly ascribed to the increase of surface area and surface oxidation induced by mechanical activation. This work provides novel insights into the improvement of catalytic performance of natural minerals by mechanical activation.

Key words: advanced oxidation process; chalcopyrite; mechanical activation; natural minerals; tetracycline

Cite this article as: WANG Chong-qing, YANG Jia-peng, HUANG Rong, CAO Yi-jun. Mechanical activation of natural chalcopyrite for improving heterogeneous Fenton degradation of tetracycline [J]. Journal of Central South University, 2022, 29(12): 3884−3895. DOI: https://doi.org/10.1007/s11771-022-5199-y.

1 Introduction

Environment problems resulted from wastewater pollution become a critical issue. Emerging organic pollutants such as antibiotics, pesticides, endocrine disruptors, pharmaceuticals and personal care products in wastewater manifest high bio-toxicity or ecological effects. For example, antibiotics induce an increase in resistant bacteria, changing the microbial structure and community of the ecosystem and disrupting the ecosystem balance [1]. Numerous techniques such as adsorption [2], coagulation [3], and membrane separation [4] are developed for wastewater remediation. Among these technologies, advanced oxidation processes (AOPs) are highly promising for application due to strong oxidizing ability, high efficiency, and easy operation.

In the past decade, heterogeneous Fenton processes are extensively studied to conquer the disadvantage of traditional Fenton processes such as incapable catalyst recovery, narrow pH, and generating massive iron sludge [5]. The development of efficient and cost-effective catalysts still limits heterogeneous Fenton processes. Various iron-based catalysts have been proposed for efficient degradation of organic pollutants. Iron oxides such as magnetite, goethite, lepidocrocite, hematite, and ferrihydrite can induce H_2O_2 activation for radical generation, causing the degradation of organic pollutants [6]. Zero-valent iron as inexpensive, green, and reactive catalyst

Foundation item: Project(2020YFC1908802) supported by the National Key Research and Development Project of China
Received date: 2022-05-02; **Accepted date:** 2022-06-01
Corresponding author: CAO Yi-jun, PhD, Professor; E-mail: yijuncao@126.com; ORCID: https://orcid.org/0000-0002-8612-3655

have been widely reported in heterogeneous Fenton process [7]. Iron compounds such as ferrites and iron-based metal-organic framework are investigated as potential catalysts [8−9]. Immobilization of iron species on porous supports, such as clay [10], zeolite [11], activated carbon [12], N-doped porous carbon [13], is an important strategy to improve catalytic ability and increase atom economy. Currently, the catalysts still suffer from drawbacks such as complex synthesis, high cost, and low efficiency.

Numerous iron minerals are studied as heterogeneous Fenton catalysts for removing a variety of organic pollutants, owing to low cost, natural abundance, and environmental friendliness. Hematite catalyzed Fenton discoloration of Orange G was investigated, and the degradation at 60 min reached 95.14% under conditions of 20 g/L catalyst, 800 mg/L H_2O_2, pH 3.0, and temperature 25 ℃ [14]. Antibiotics removal in simulated and real wastewater was examined in the presence of H_2O_2 and natural magnetite, and 100% removal of sulfamethoxazole was obtained at 240 min under proper conditions [15]. ZHANG et al [16] studied the catalytic performance, degradation kinetics, and reaction mechanism for carmine removal in siderite/H_2O_2 system. A strategy of pre-reaction between natural pyrite and H_2O_2 was proposed for improving catalytic degradation of dyes [17]. Chalcopyrite ($CuFeS_2$), a copper-iron sulfide mineral existing in the earth's crust, can be a promising heterogeneous Fenton catalyst. The availability of Cu and Fe in the mineral may manifest synergic action to stimulate H_2O_2 activation and thus generate more reactive hydroxyl radical. Additionally, the oxidation of reduced sulfur species in chalcopyrite promotes Cu^{2+}/Cu^{+} and Fe^{3+}/Fe^{2+} cycle and the self-regulation of solution pH [18−19]. Catalyzed Fenton degradation of organic pollutants is rarely reported using natural chalcopyrite. Chalcopyrite from different mineral sources differs significantly such as mineral composition, surface structure, and crystal defects. HUANG et al [18] found that the chalcopyrite type affected heterogeneous Fenton degradation of acid Orange 7. Generally, natural minerals display low catalytic performance compared to well-designed catalysts, and it is imperative to develop efficient methods to improve the catalytic ability of natural minerals. Mechanical activation as an effective strategy to regulate mineral surface is widely used in mineral flotation and mineral leaching [20−21]. To the best of our knowledge, less reports on mechanical activation of chalcopyrite are available for improving catalytic performance.

This study conducted an explorative research on the enhancement of catalytic ability of natural mineral by mechanical activation. The catalytic performance of natural chalcopyrite after mechanical activation was compared for antibiotic degradation. Multiple characterizations were conducted to reveal the property change of chalcopyrite caused by mechanical activation. The tentative mechanism of mechanical activation was revealed.

2 Materials and methods

2.1 Materials

Natural chalcopyrite with a purity larger than 95% was obtained from a local copper mine in Hubei province, China. Mechanical activation of chalcopyrite was conducted for milling different time (10, 30, 60 and 120 min), particles less than 0.075 mm were used as catalysts, and the samples were abbreviated as Chp10, Chp30, Chp60, and Chp120, respectively. Tetracycline (TC) was used as target pollutant, and hydrogen peroxide (30%) was used as oxidant for heterogeneous Fenton reaction. Tert-butyl alcohol (TBA), isopropyl alcohol (IPA) and chloroform (CF) were used as radical scavengers. Chemicals used in experiments were analytically pure.

2.2 Catalysis

Typically, chalcopyrite samples and H_2O_2 were added into 50 mL TC solution (40 mg/L) in Erlenmeyer flask. The flask was put in a thermostatic oscillator at 150 r/min. After oscillation for certain time, solution sample was taken out, centrifuged for 1 min, and determined at 357 nm by the ultraviolet-visible (UV-vis) spectrophotometer. The degradation was calculated by Eq. (S1). The effects of TBA, IPA and CF on TC degradation were studied to clarify the role of radical species.

2.3 Characterizations

The surface area was determined using an ASAP 2020 surface area analyzer (Micromeritics) through N_2 adsorption/desorption at 77 K. The morphology and the elements were examined by a Quanta FEG 250 scanning electron microscope (SEM; FEI) and an energy dispersive X-ray spectroscope (EDX). An ultimate IV X-ray diffraction spectroscope (XRD; Rigaku) was employed to examine the crystalline structure of chalcopyrite samples. The surface elements were measured under an ESCALAB 250XI X-ray photoelectron spectroscope (XPS; Thermo Scientific). The particle distribution of chalcopyrite was recorded using a Mastersizer 2000 laser diffraction particle size analyzer (Marvin). The concentration of TC solution was determined employing an UV-2600 UV-vis spectroscope (Shimadzu). A JES FA200 spectrometer (JEOL) was used to record the electron spin resonance (ESR) spectrum for identifying the hydroxyl radical.

3 Results and discussion

3.1 Tetracycline degradation

Antibiotics as emerging pollutants attract increasing worldwide attention owning to serious threats to humans and animals [1]. Tetracycline as human and veterinary medicine is one of the most widely used antibiotics, and its release into wastewater causes adverse effects on the ecological system and public health [22]. Tetracycline has been widely reported as target pollutant in heterogeneous Fenton process [5]. To examine the effect of mechanical activation on the catalytic performance of natural chalcopyrite, chalcopyrite samples with different milling time were prepared. TC degradation was conducted in the presence of H_2O_2 and chalcopyrite (Chp10, Chp30, Chp60, and Chp120). The variation of TC concentration during catalytic process is shown in Figure 1(a). Gradual decline of TC concentration is observed with

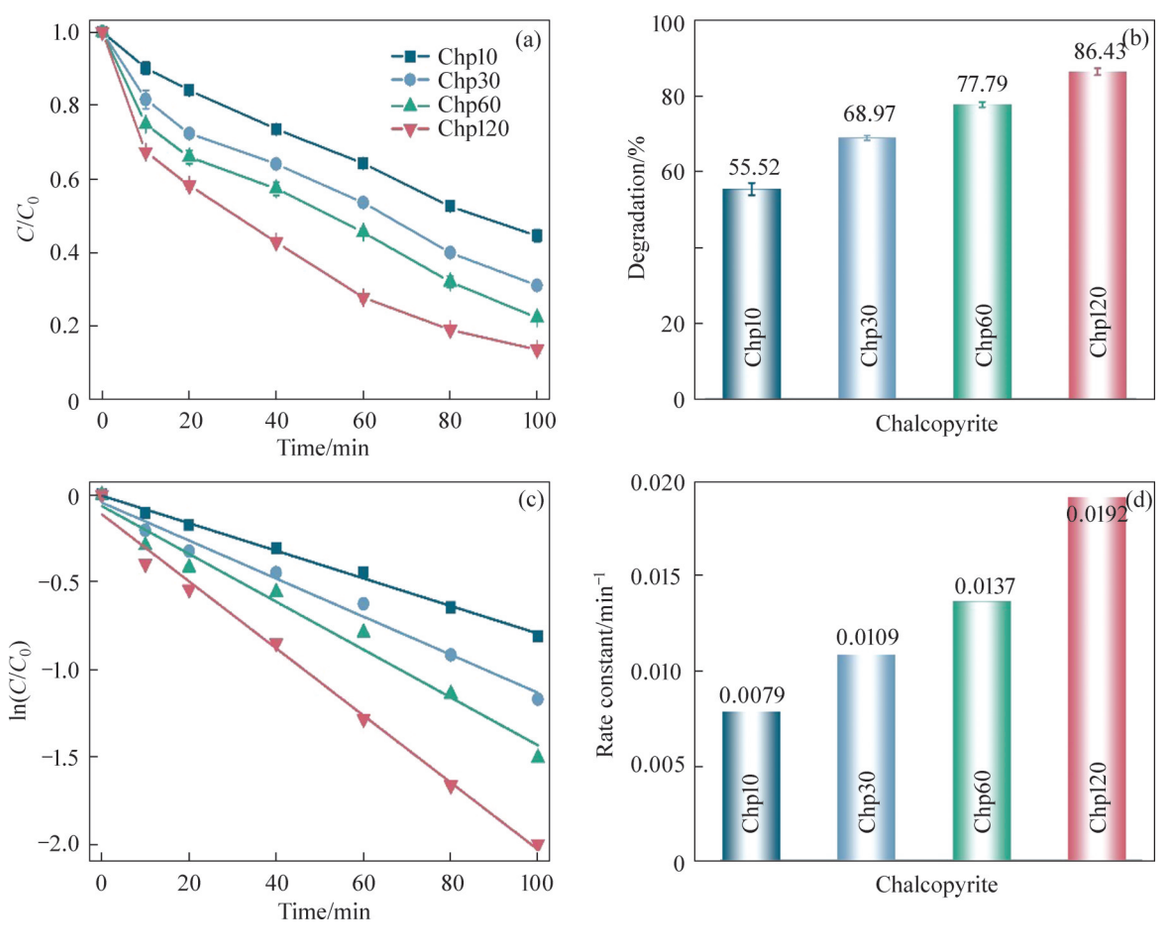

Figure 1 (a) Change of tetracycline concentration as a function of reaction time; (b) Tetracycline degradation in 100 min; (c) The linear fitting of pseudo-first-order kinetics; (d) The rate constant of Tetracycline degradation (Experimental conditions: 2 g/L chalcopyrite, 0.04 mol/L H_2O_2, 40 mg/L tetracycline, temperature 25 °C)

increasing reaction time, suggesting the good catalytic ability of chalcopyrite as heterogeneous Fenton catalyst [23]. A difference exists in the degradation behavior among chalcopyrite samples, and the catalytic performance obeys the sequence: Chp10<Chp30<Chp60<Chp120. The decline of TC concentration for Chp120 is more significant than that of Chp10. TC degradation at 100 min is 55.52%, 68.97%, 77.79% and 86.43% for Chp10, Chp30, Chp60, and Chp120, respectively (Figure 1(b)).

Kinetics analysis offers insights into catalytic process of TC degradation [24]. In heterogeneous Fenton process, hydroxyl radical is the major oxidative species for pollutant degradation. The •OH concentration in catalytic system depends on: 1) the reactions between •OH and TC; 2) the reactions between H_2O_2 and active metals in chalcopyrite; and 3) the reactions between •OH and radical scavengers such as reactive oxygen species [25]. On the assumption of reaction equilibrium, the time-invariant •OH concentration, and the presence of a great amount of scavenger species over TC concentration [26], TC degradation can be described by pseudo-first-order kinetics (details are described in Text S2).

Figure 1(c) shows the results of linear fitting of kinetic model. The rate constant for TC degradation is 0.0079, 0.0109, 0.0137 and 0.0192 min^{-1} for Chp10, Chp30, Chp60, and Chp120, respectively (Figure 1(d)). The reaction rate for TC degradation is significantly improved with increasing milling time of chalcopyrite. Therefore, mechanical activation is effective to improve the catalytic ability of natural chalcopyrite. The improvement associated with mechanical activation may be ascribed to: 1) the variation of surface area or particle size; 2) the transformation of mineral structure; 3) elemental change of chalcopyrite [27−28]. Multiple characterizations are implemented to reveal the potential mechanism.

3.2 Surface area and particle size

The surface area of chalcopyrite was determined by the N_2 adsorption isotherms. From Figure 2(a), type II isotherm are observed with minor hysteresis loop, suggesting the non-porous structure of chalcopyrite. The pore structure can be characterized by Figure 2(a_1), which exhibits similar results of the existence of very limited nano pores. The BET surface area of Chp10, Chp30, Chp60 and Chp120 is 1.14, 1.23, 1.28 and 1.42 m^2/g, respectively (Table 1). With increasing milling time, the surface area and total pore volume of chalcopyrite increase slightly. The results may be attributed to the decrease in particle size induced by mechanical effect [27].

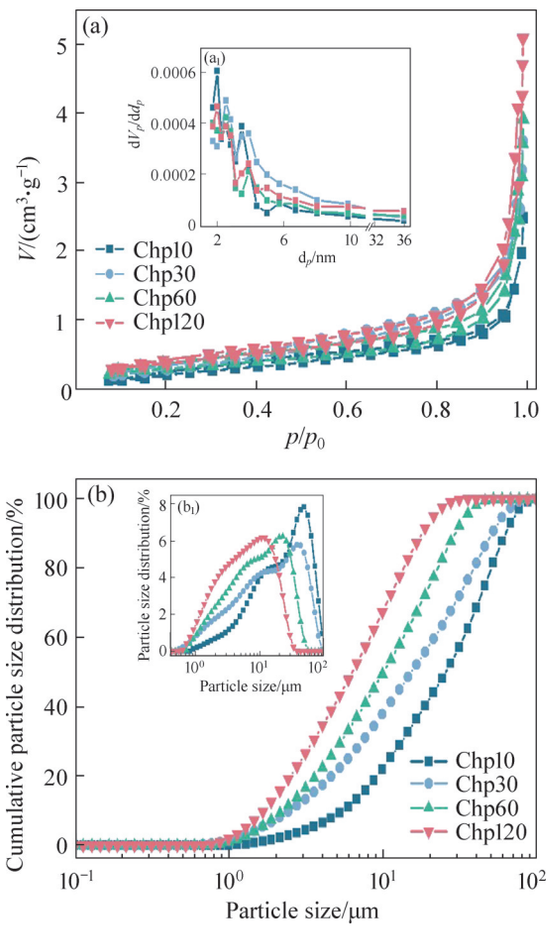

Figure 2 (a, a_1) N_2 adsorption and desorption isotherms and pore size distribution; (b, b_1) Laser grain size analysis of Chp10, Chp30, Chp60, and Chp120

Table 1 Surface area and pore structure of Chp10, Chp30, Chp60, and Chp120

Chalcopyrite sample	Specific surface area/ ($m^2 \cdot g^{-1}$)	Total pore volume/ ($cm^3 \cdot g^{-1}$)	Average pore size/nm
Chp10	1.14	0.0035	12.34
Chp30	1.23	0.0054	17.52
Chp60	1.28	0.0055	20.41
Chp120	1.42	0.0076	21.04

Laser grain size analysis was performed to examine the change of particle size of chalcopyrite under mechanical activation. Figure 2(b) manifests that the particle size of chalcopyrite is mainly between 1 and 100 μm. Cumulative particle size distribution increases more rapidly to 100% with increasing milling time. From Figure 2(b_1), it can be seen that the particle size of Chp10 is mainly larger than 10 μm. Comparatively, there are more particles less than 10 μm for Chp30, Chp60 and Chp120. The decline in particle size can be further verified by the variation of granulometric parameters including D_{10}, D_{50} and D_{90} (volume moment mean diameter). The granulometric parameters of chalcopyrite decrease obviously from Chp10 to Chp120 (Table 2). The value of D_{50} is declined from 25.4 to 6.3 μm. The results are consistent with previous study by ZHAO et al [27].

Table 2 Changes of particle size of Chp10, Chp30, Chp60, and Chp120

Chalcopyrite sample	D_{10}/μm	D_{50}/μm	D_{90}/μm
Chp10	5.4	25.4	62.0
Chp30	2.5	15.2	50.6
Chp60	2.2	10.0	29.2
Chp120	1.7	6.3	17.8

3.3 SEM and EDX analysis

SEM was used to directly observe the micro-morphology and particles of chalcopyrite. Figure S1 shows the irregular size and shape of chalcopyrite particles. There are many large particles with smooth surface for Chp10. Figure 3(a) manifests a few small particles attached on the surface of large particles. Figure 3(b) shows that the presence of more small particles resulted from the milling of large particle for Chp30. With increasing milling time, the particle size of chalcopyrite becomes smaller (Figures 3(c) and (d)). For Chp60 and Chp120, it can be clearly observed that many small particles are closely attached, forming particle agglomeration [27]. For Chp120, the existence of nano particles can be observed (Figure S2). The transformation of the bulk structure of chalcopyrite particles into layered structure occurs during mechanical activation [21]. EDX spectrum exhibits the presence of iron, copper, and sulfur as major elements, indicating $CuFeS_2$ mineral in natural chalcopyrite.

3.4 XRD analysis

XRD patterns of chalcopyrite samples are shown in Figure 4. The main phase of $CuFeS_2$ mineral can be clearly observed in natural chalcopyrite. The XRD peaks at 29.4°, 33.9°, 34.4°, 48.6°, 49.0°, 57.8° and 58.5° correspond to the planes of (1 1 2), (2 0 0), (0 0 4), (2 2 0), (3 1 2) and (1 1 6) of $CuFeS_2$ (PDF#99-0029), respectively [29−30]. The sharp peaks for Chp10 indicate the good crystallinity of inherent $CuFeS_2$ in chalcopyrite. No obvious peak shift is seen after mechanical activation. Gradual broadening of the peaks occurs associated with prolonging milling time. The full width at half maximum (FWHM) of main peak (1 1 2) is 0.1750°, 0.1789°, 0.2151° and 0.2242° for Chp10, Chp30, Chp60 and Chp120, respectively. This is ascribed to the decline in grain size, the induced lattice strain, and the accumulation of amorphization [27]. A few minor peaks at 28.5° , 33.1°, 37.1°, 47.4° and 56.3° appear with increasing milling time, and they are assigned to the planes of (1 1 1), (2 0 0), (2 1 0) and (3 1 1) of pyrite (PDF#42-1340), respectively [31]. This can be attributed to the formation of FeS_2 due to phase transformation (Reaction (1)) during mechanical activation [28].

$$CuFeS_2+O_2 \rightarrow CuO+FeS_2 \quad (1)$$

3.5 XPS analysis

Figure S3 displays the full XPS spectra of Chp10, Chp30, Chp60, and Chp120. For all chalcopyrite samples, the spectra manifest the peaks at the binding energy of around 162, 532, 712 and 932 eV, assigning to S 2p, O 1s, Fe 2p amd Cu 2p, respectively. The existence of S, Cu, and Fe elements is attributed to $CuFeS_2$. From Chp10 to Chp120, the O content increases gradually from 24.26% to 35.67%, indicating the oxidation of chalcopyrite with increasing milling time (Table 3). No metal oxides are identified by XRD analysis, suggesting that the induced oxidation by mechanical activation probably occurs on chalcopyrite surface and generates low content of amorphous oxidation products [21].

The high-resolution XPS spectra of S 2p, O 1s, Fe 2p and Cu 2p are shown in Figure 5. The high-resolution S 2p spectra can be fitted by four peaks at binding energy of around 161.4, 162.5, 163.9 and

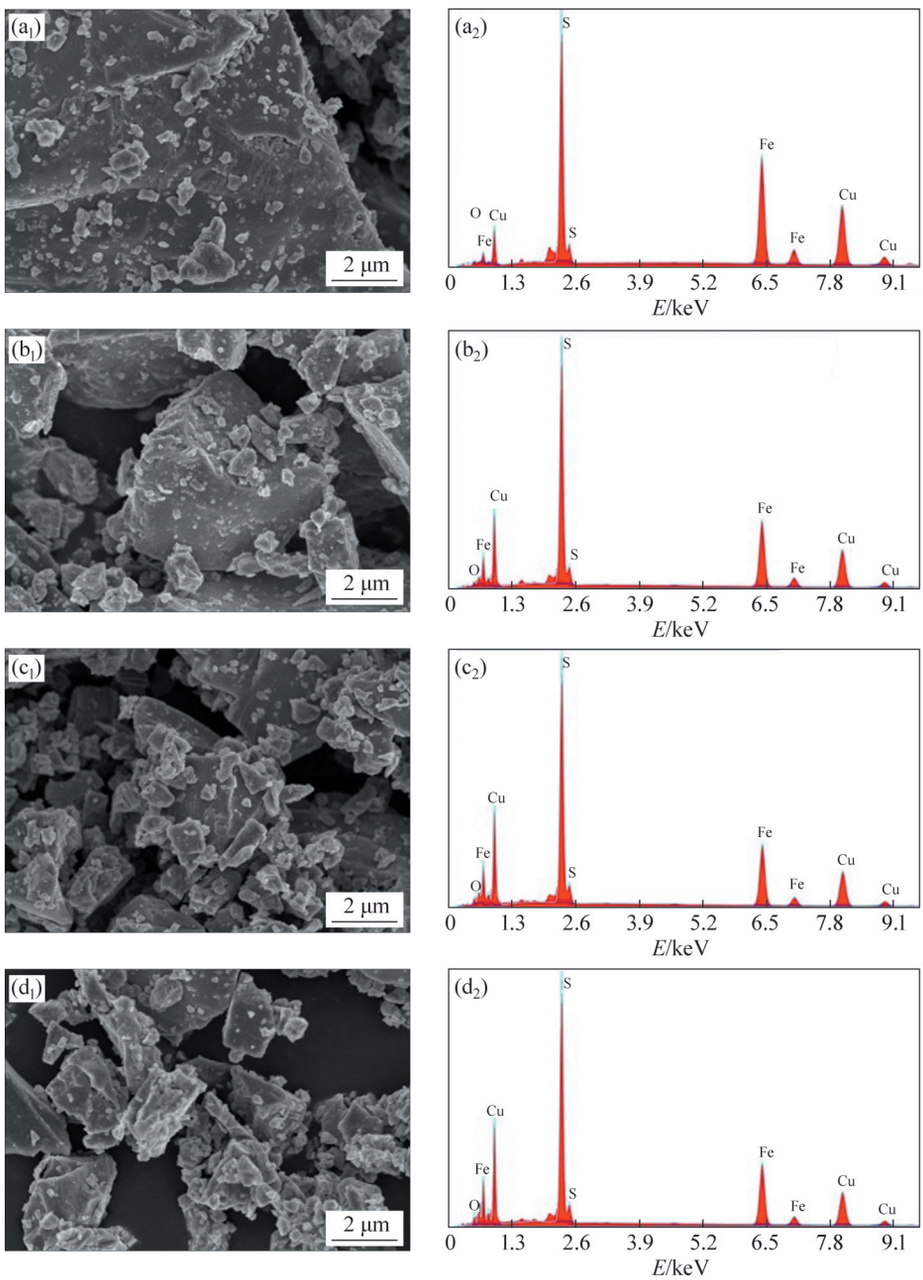

Figure 3 SEM images and EDX spectra of (a) Chp10, (b) Chp30, (c) Chp60 and (d) Chp120

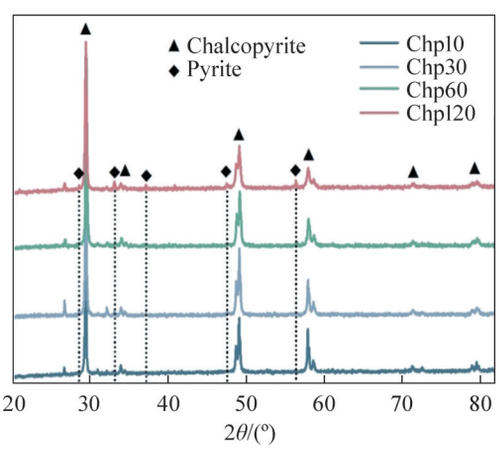

Figure 4 XRD patterns of chalcopyrite samples

Table 3 Relative atomic content of elements in chalcopyrite at%

Chalcopyrite sample	S	O	Fe	Cu
Chp10	35.43	24.26	18.39	21.92
Chp30	33.00	28.72	18.08	20.20
Chp60	32.28	29.96	18.17	19.59
Chp120	29.74	35.67	16.89	17.71

169.2 eV, which are assigned to monosulfide (S^{2-}), disulfide (S_2^{2-}), polysulfide (S_n^{2-}), and sulfate (SO_4^{2-}), respectively [17, 32]. The intensity of peak ascribed to S^{2-} decreases obviously, while that of S_n^{2-} and

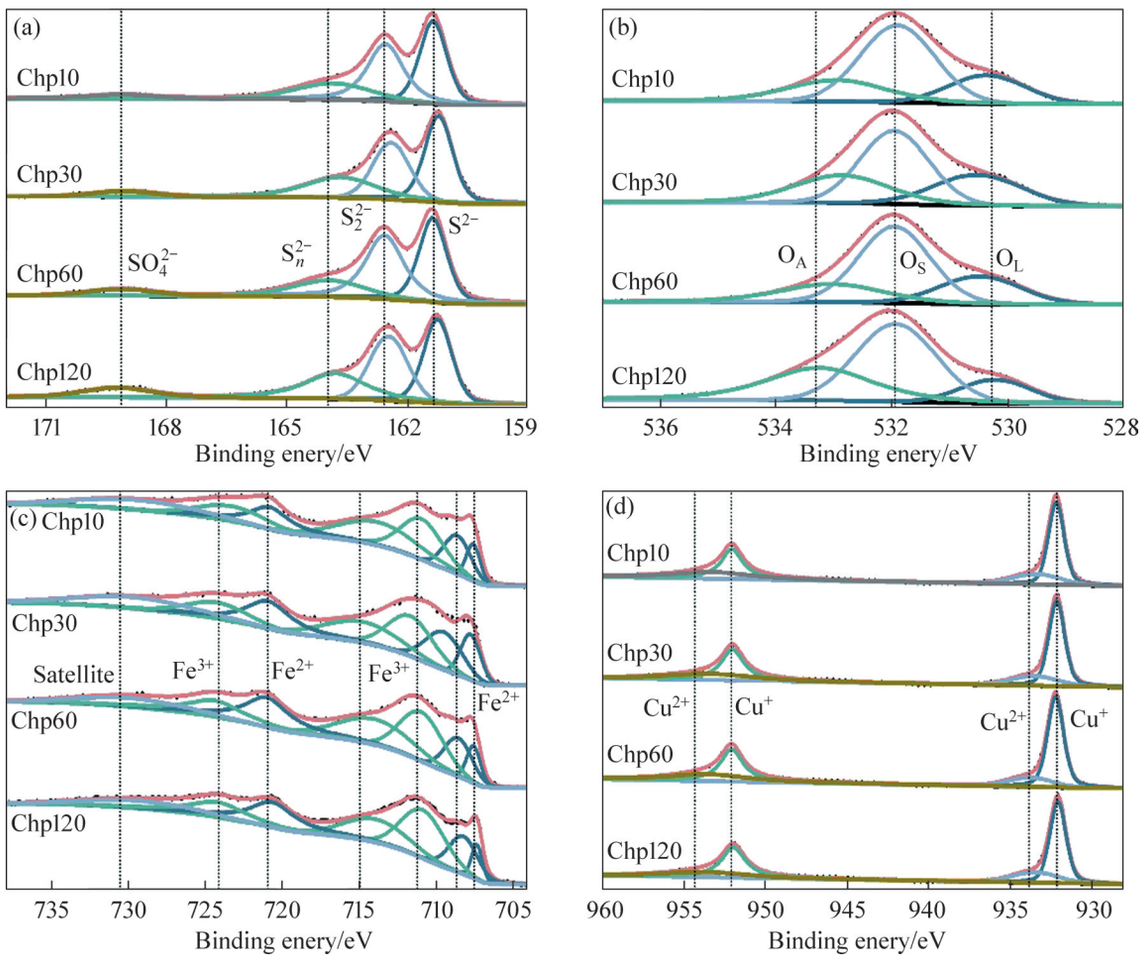

Figure 5 High-resolution XPS spectra of Chp10, Chp30, Chp60 and Chp120: (a) S 2p; (b) O 1s; (c) Fe 2p; (d) Cu 2p

SO_4^{2-} increases gradually with prolonging milling time (Table S3). The results manifest the oxidation of sulfur species, and S^{2-} is transformed into S_n^{2-} and SO_4^{2-} during mechanical activation. This agrees well with the increase of O content of chalcopyrite samples. For high-resolution O 1s spectra, three peaks at binding energy of around 530.4, 531.9 and 533.0 eV, are assigned to lattice oxygen (O_L), surface oxygen (O_S), and adsorbed oxygen (O_A) [33]. No significant change of oxygen species occurs for different chalcopyrite samples.

The high-resolution Fe 2p spectra exhibit the peaks assigned to Fe $2p_{3/2}$ (around 710 eV) and Fe $2p_{1/2}$ (around 722 eV). Peak fitting of Fe $2p_{3/2}$ displays peaks at around 707.6 eV (Fe^{2+}), 708.6 eV (Fe^{2+}), 711.2 eV (Fe^{3+}), and 714.8 eV (Fe^{3+}) [17]. The peak of Fe $2p_{1/2}$ can be fitted by peaks at 720.8 eV (Fe^{2+}) and 723.3 eV (Fe^{3+}) [34]. No significant variation of Fe 2p peaks occurs for the chalcopyrite samples. The sharp peaks at binding energy of around 932.2 eV and 952.1 eV are ascribed to Cu $2p_{3/2}$ and Cu $2p_{1/2}$ [34]. The two Cu 2p peaks can be fitted by peaks assigned to Cu^+ and Cu^{2+}. No obvious increase or decrease of the peaks is seen associated with milling time. Therefore, mechanical activation mainly results in partial oxidation of sulfur species in chalcopyrite [21].

3.6 Mechanism of mechanical activation

According to above analyses, mechanical activation of natural chalcopyrite induces the decline of particle size, slight increase of surface area, smaller grain size, lattice strain, and partial oxidation of sulfur species. All these changes may be related to the catalytic activity of chalcopyrite. To clarify the mechanism of mechanical activation for improving catalytic performance, the relationship between catalytic activity and property change is investigated. The rate constant is regarded as the indicator of catalytic activity of chalcopyrite.

Typical parameters of surface area, particle size, crystalline structure, and surface element are designated as BET surface area, granulometric parameter D_{50}, FWHM of typical XRD peak, and relative content of surface oxygen. The results of linear relationship are exhibited in Figure 6. Catalytic ability displays positive correlation with surface area, the FWHM, and oxygen content, and it manifests negative correlation with D_{50}. In addition, the rate constant has a good linear relationship with surface area and oxygen content due to a high correlation coefficient (R^2>0.96). It can be deduced that the improved catalytic ability of chalcopyrite is mainly ascribed to the increase of surface area and surface oxidation induced by mechanical activation.

The generation of dominant hydroxyl radical is clarified by quenching experiments and EPR determination. In heterogeneous Fenton process, hydroxyl radical is dominant reactive oxygen species for pollutant degradation. TBA, IPA, and CF are common scavengers for hydroxyl radical and superoxide radicals [5]. Comparison of TC degradation in the presence of TBA, IPA, and CF is shown in Figure S4. Significant decline in TC degradation is observed with the addition of TBA and IPA, manifesting the important role of hydroxyl radical in TC degradation [35]. Figure S5 exhibits EPR spectra of H_2O_2 and H_2O_2/chalcopyrite system. No special peak is seen in the presence of only H_2O_2. The peak with an intensity ratio of 1:2:2:1 is attributed to the DMPO-·OH adduct in H_2O_2/chalcopyrite system [33, 36]. Copper and iron in chalcopyrite are reactive metals for H_2O_2 activation and the generation of hydroxyl radical. Chalcopyrite reacts with H_2O_2 to produce Fe^{3+} and Cu^{2+} (Reaction (2)). Cu^{2+} can be converted to Cu^{+} via Reaction (3), and Fe^{3+} is transformed to Fe^{2+} through Reaction (4). The generation of •OH induced by Cu^{+} and Fe^{2+} can be shown as Reactions (5) and (6). Moreover, the sulfur species may contribute to the reduction of Fe^{3+} and Cu^{2+} [37]. The produced •OH results in the degradation and probably

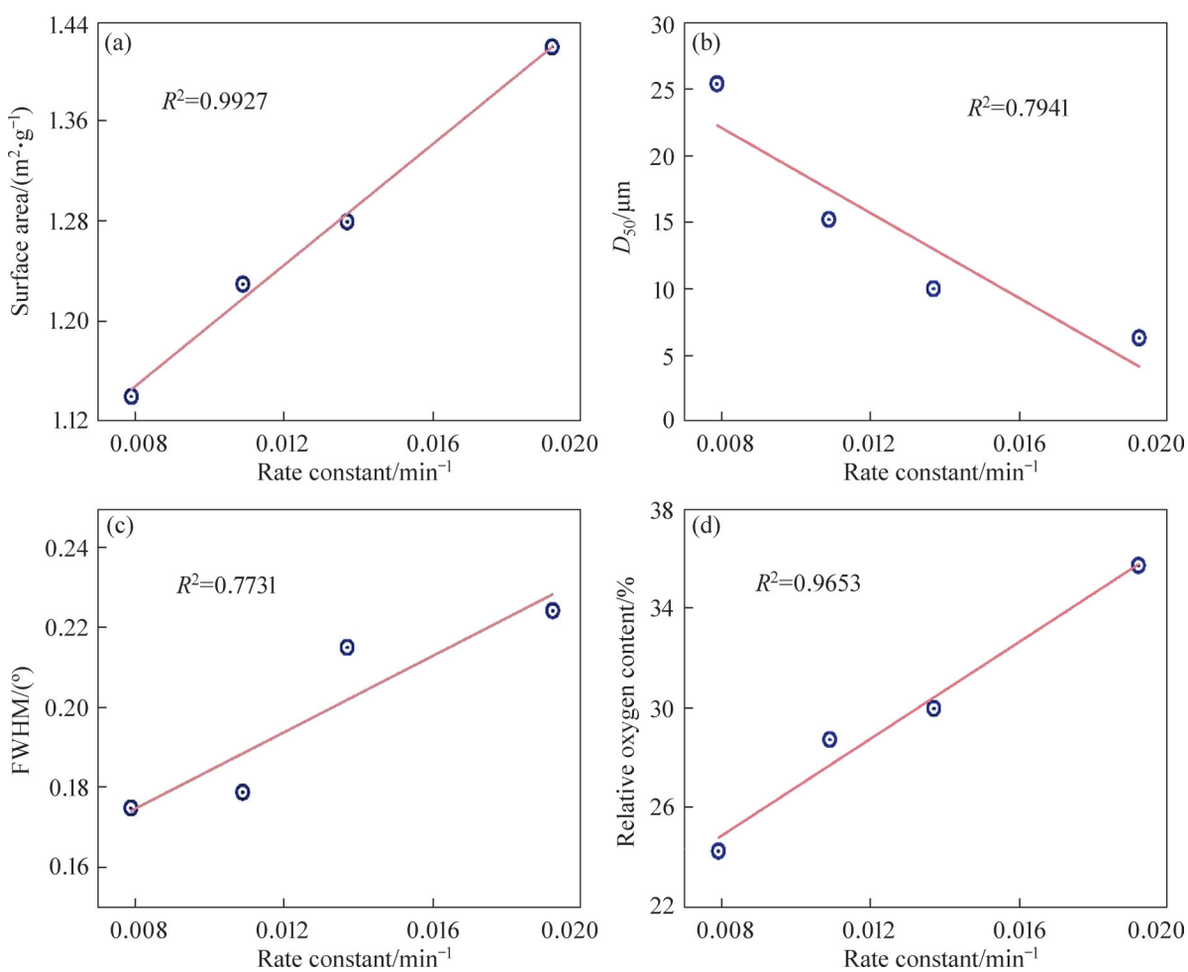

Figure 6 Linear relationship between rate constant and (a) surface area, (b) D_{50}, (c) FWHM, and (d) relative oxygen content

mineralization of TC molecules (Reaction (7)). More efforts should be conducted to get in-depth understanding of the role of specific sites such as metal components and sulfur vacancies [38−39].

$$CuFeS_2+H_2O_2\rightarrow Fe^{3+}+Cu^{2+}+SO_4^{2-}+H_2O+H^+ \quad (2)$$

$$Cu^{2+}+H_2O_2\rightarrow Cu^{+}+HO_2\bullet+H^+ \quad (3)$$

$$Fe^{3+}+H_2O_2\rightarrow Fe^{2+}+\bullet O_2^{-}+H^+ \quad (4)$$

$$Cu^{+}+H_2O_2\rightarrow Cu^{2+}+\bullet OH+OH^- \quad (5)$$

$$Fe^{2+}+H_2O_2\rightarrow Fe^{3+}+\bullet OH+OH^- \quad (6)$$

$$C_{22}H_{24}N_2O_8+H_2O_2\rightarrow CO_2+H_2O+H+NO_3^- \quad (7)$$

4 Conclusions

1) The catalytic performance obeys the sequence: Chp10<Chp30<Chp60<Chp120. The rate constants of pseudo-first-order kinetics for TC degradation are 0.0079, 0.0109, 0.0137 and 0.0192 min^{-1} for Chp10, Chp30, Chp60 and Chp120, respectively. Mechanical activation induces obvious improvement of catalytic performance of natural chalcopyrite.

2) The change of natural chalcopyrite resulted from mechanical activation is revealed by multiple characterizations. Mechanical activation of natural chalcopyrite induces the decline of particle size, slight increase of surface area, smaller grain size, lattice strain, and partial oxidation of sulfur species.

3) The relationship between catalytic activity and properties changes manifests that the improved catalytic ability is mainly ascribed to the increase of surface area and surface oxidation induced by mechanical activation.

4) Mechanical activation can be a promising method for improving catalytic performance of natural minerals.

Appendix

Text S1

The degradation was calculated by Eq. (S1). The effects of TBA, IPA and CF on TC degradation were studied to clarify the role of radical species.

$$D=(C_0-C)/C_0 \quad (S1)$$

where D is the tetracycline degradation; C_0 and C is the initial and final tetracycline concentration (mg/L), respectively.

Text S2

In heterogeneous Fenton process, hydroxyl radical is the major oxidative species for pollutant degradation. The rate equation of tetracycline degradation can be expressed as Eq. (S2). The •OH concentration in catalytic system depends on: 1) the reactions between •OH and TC; 2) the reactions between H_2O_2 and active metals in chalcopyrite; and 3) the reactions between •OH and radical scavengers such as reactive oxygen species. The rate equation for •OH can be depicted in Eq. (S3).

$$d[TC]/dt=-k_1[\bullet OH][TC] \quad (S2)$$

$$d[\bullet OH]/dt=k_2[H_2O_2][Chp]-k_3[\bullet OH][TC]-\sum_j k_j[RS][\bullet OH] \quad (S3)$$

where k_1, k_2 and k_3 are the rate constants; Chp and RS represent chalcopyrite and radical scavengers, respectively.

On the assumption of reaction equilibrium, the •OH concentration is time-invariant, and Eq. (S4) is obtained. Combining Eqs. (S2) − (S5), due to the presence of a great amount of scavenger species in catalytic system, it can be assumed that k_3[TC] is significantly smaller than $\sum_j k_j$[RS]. Then, Eq. (S5) can be transformed into Eq. (S6). Therefore, TC degradation can be described by pseudo-first-order kinetics.

$$d[\bullet OH]/dt=0 \quad (S4)$$

$$d[TC]/dt=-k_1[TC](k_2[H_2O_2][Chp])/(k_3[TC]+\sum_j k_j[RS]) \quad (S5)$$

$$d[TC]/dt=-k_2[TC](k_2[H_2O_2][Chp])/\sum_j k_j[RS]=-k_a[TC] \quad (S6)$$

where k_a is the apparent rate constant of pseudo-first-order kinetics.

Table S1 The relative content of sulfur species in chalcopyrite wt%

Chalcopyrite sample	S^{2-}	S_2^{2-}	S_n^{2-}	SO_4^{2-}
Chp10	36.23	37.94	19.81	6.02
Chp30	35.76	33.67	23.59	6.98
Chp60	34.83	31.26	26.97	6.94
Chp120	32.01	30.44	27.75	9.80

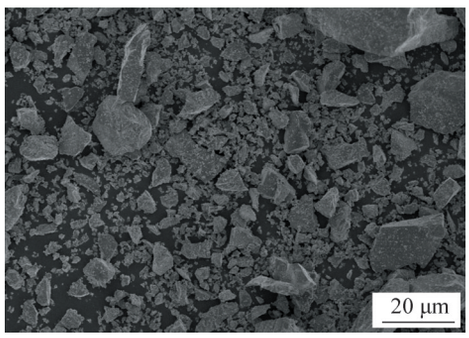

Figure S1 SEM image of Chp10

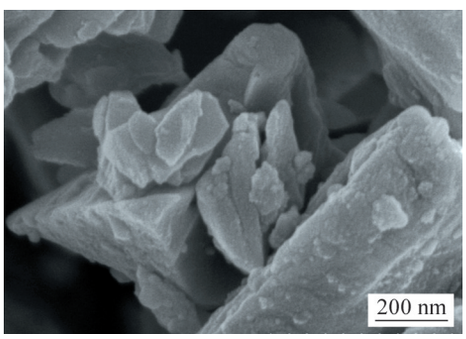

Figure S2 SEM image of Chp120

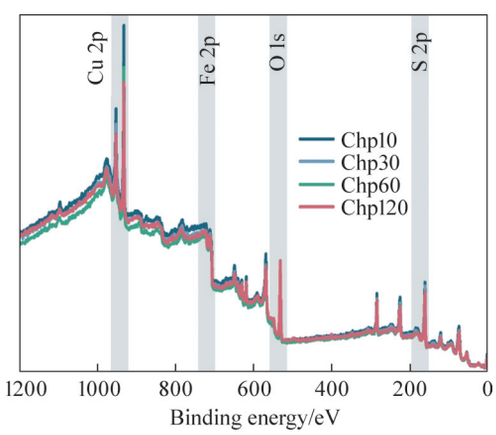

Figure S3 Full XPS spectrum of Chp10, Chp30, Chp60, and Chp120

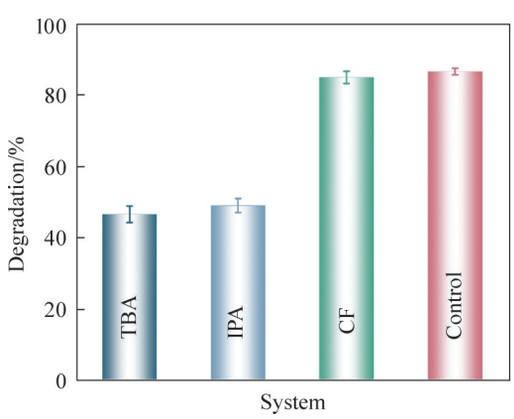

Figure S4 Effect of radical scavengers on tetracycline degradation

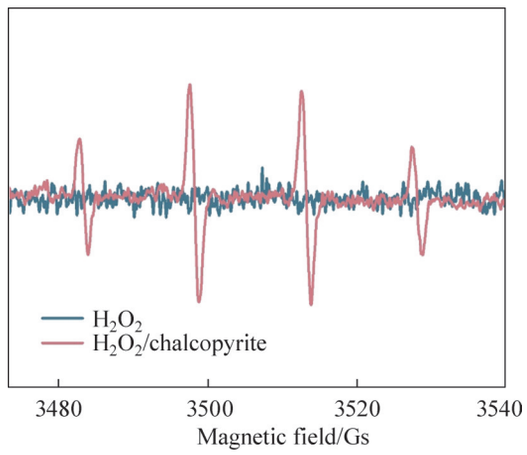

Figure S5 EPR spectrum of DMPO-trapped hydroxyl radical

Contributors

The overarching research goals were developed by WANG Chong-qing and CAO Yi-jun. YANG Jia-peng and HUANG Rong conducted experimental studies and analyzed the experimental results. The initial draft of the manuscript was written by WANG Chong-qing. YANG Jia-peng, HUANG Rong and CAO Yi-jun edited the draft of manuscript. All authors replied to reviewers' comments and revised the final version.

Conflict of interest

WANG Chong-qing, YANG Jia-peng, HUANG Rong and CAO Yi-jun declare that they have no conflict of interest.

References

[1] GARCÍA J, GARCÍA-GALÁN M J, DAY J W, et al. A review of emerging organic contaminants (EOCs), antibiotic resistant bacteria (ARB), and antibiotic resistance genes (ARGs) in the environment: Increasing removal with wetlands and reducing environmental impacts [J]. Bioresource Technology, 2020, 307: 123228. DOI: 10.1016/j.biortech.2020.123228.

[2] AWAD A M, SHAIKH S M R, JALAB R, et al. Adsorption of organic pollutants by natural and modified clays: A comprehensive review [J]. Separation and Purification Technology, 2019, 228: 115719. DOI: 10.1016/j.seppur.2019.115719.

[3] ZHAO Chuan-liang, ZHOU Jun-yuan, YAN Yi, et al. Application of coagulation/flocculation in oily wastewater treatment: A review [J]. Science of the Total Environment, 2021, 765: 142795. DOI: 10.1016/j.scitotenv.2020.142795.

[4] PAN Zong-lin, SONG Cheng-wen, LI Lin, et al. Membrane technology coupled with electrochemical advanced oxidation

processes for organic wastewater treatment: Recent advances and future prospects [J]. Chemical Engineering Journal, 2019, 376: 120909. DOI: 10.1016/j.cej.2019.01.188.

[5] WANG Chong-qing, SUN Rui-rui, HUANG Rong, et al. Superior Fenton-like degradation of tetracycline by iron loaded graphitic carbon derived from microplastics: Synthesis, catalytic performance, and mechanism [J]. Separation and Purification Technology, 2021, 270: 118773. DOI: 10.1016/j.seppur.2021.118773.

[6] ZHAO Ling, LIN Zhi-rong, MA Xiao-hong, et al. Catalytic activity of different iron oxides: Insight from pollutant degradation and hydroxyl radical formation in heterogeneous Fenton-like systems [J]. Chemical Engineering Journal, 2018, 352: 343−351. DOI: 10.1016/j.cej.2018.07.035.

[7] KAKAVANDI B, TAKDASTAN A, POURFADAKARI S, et al. Heterogeneous catalytic degradation of organic compounds using nanoscale zero-valent iron supported on kaolinite: Mechanism, kinetic and feasibility studies [J]. Journal of the Taiwan Institute of Chemical Engineers, 2019, 96: 329−340. DOI: 10.1016/j.jtice.2018.11.027.

[8] JOSEPH J, IFTEKHAR S, SRIVASTAVA V, et al. Iron-based metal-organic framework: Synthesis, structure and current technologies for water reclamation with deep insight into framework integrity [J]. Chemosphere, 2021, 284: 131171. DOI: 10.1016/j.chemosphere.2021.131171.

[9] SOUFI A, HAJJAOUI H, ELMOUBARKI R, et al. Spinel ferrites nanoparticles: Synthesis methods and application in heterogeneous Fenton oxidation of organic pollutants—A review [J]. Applied Surface Science Advances, 2021, 6: 100145. DOI: 10.1016/j.apsadv.2021.100145.

[10] IOFFE M, KUNDU S, PEREZ-LAPID N, et al. Heterogeneous Fenton catalyst based on clay decorated with nano-sized amorphous iron oxides prevents oxidant scavenging through surface complexation [J]. Chemical Engineering Journal, 2022, 433: 134609. DOI: 10.1016/j.cej.2022.134609.

[11] AYOUB H, ROQUES-CARMES T, POTIER O, et al. Iron-impregnated zeolite catalyst for efficient removal of micropollutants at very low concentration from Meurthe River [J]. Environmental Science and Pollution Research, 2018, 25(35): 34950 − 34967. DOI: 10.1007/s11356-018-1214-0.

[12] RAJI M, MIRBAGHERI S A, YE Fei, et al. Nano zero-valent iron on activated carbon cloth support as Fenton-like catalyst for efficient color and COD removal from melanoidin wastewater [J]. Chemosphere, 2021, 263: 127945. DOI: 10.1016/j.chemosphere.2020.127945.

[13] YANG Wu, HONG Pei-dong, YANG Dan-dan, et al. Enhanced Fenton-like degradation of sulfadiazine by single atom iron materials fixed on nitrogen-doped porous carbon [J]. Journal of Colloid and Interface Science, 2021, 597: 56−65. DOI: 10.1016/j.jcis.2021.03.168.

[14] GHIME D, MAHAJAN J, GHOSH P. Decoloration of Orange G by mineral hematite catalyzed Fenton-like process [J]. Environmental Engineering Science, 2016: ees.2015.0534. DOI: 10.1089/ees.2015.0534.

[15] MUNOZ M, CONDE J, de PEDRO Z M, et al. Antibiotics abatement in synthetic and real aqueous matrices by H_2O_2/natural magnetite [J]. Catalysis Today, 2018, 313: 142 − 147. DOI: 10.1016/j.cattod.2017.10.032.

[16] ZHANG Ya-qing, CHEN Tian-hu, ZHAO Yue-ling, et al. Catalytic effect of siderite on H_2O_2 oxidation of carmine dye: Performance, mechanism and kinetics [J]. Applied Geochemistry, 2019, 106: 26 − 33. DOI: 10.1016/j.apgeochem.2019.04.022.

[17] WANG Chong-qing, SUN Rui-rui, HUANG Rong, et al. A novel strategy for enhancing heterogeneous Fenton degradation of dye wastewater using natural pyrite: Kinetics and mechanism [J]. Chemosphere, 2021, 272: 129883. DOI: 10.1016/j.chemosphere.2021.129883.

[18] HUANG Xiao-tao, ZHU Tong-he, DUAN Wei-jian, et al. Comparative studies on catalytic mechanisms for natural chalcopyrite-induced Fenton oxidation: Effect of chalcopyrite type [J]. Journal of Hazardous Materials, 2020, 381: 120998. DOI: 10.1016/j.jhazmat.2019.120998.

[19] DROGUETT C, SALAZAR R, BRILLAS E, et al. Treatment of antibiotic cephalexin by heterogeneous electrochemical Fenton-based processes using chalcopyrite as sustainable catalyst [J]. Science of the Total Environment, 2020, 740: 140154. DOI: 10.1016/j.scitotenv.2020.140154.

[20] CHELGANI S C, PARIAN M, PARAPARI P S, et al. A comparative study on the effects of dry and wet grinding on mineral flotation separation-a review [J]. Journal of Materials Research and Technology, 2019, 8(5): 5004 − 5011. DOI: 10.1016/j.jmrt.2019.07.053.

[21] YANG Hong-ying, ZHAO Su-xing, WANG Gai-rong, et al. Mechanical activation modes of chalcopyrite concentrate and relationship between microstructure and leaching efficiency [J]. Hydrometallurgy, 2022, 207: 105778. DOI: 10.1016/j.hydromet.2021.105778.

[22] XU Long-yao, ZHANG He, XIONG Ping, et al. Occurrence, fate, and risk assessment of typical tetracycline antibiotics in the aquatic environment: A review [J]. Science of the Total Environment, 2021, 753: 141975. DOI: 10.1016/j.scitotenv.2020.141975.

[23] WANG Chong-qing, WANG Hui, CAO Yi-jun. Waste printed circuit boards as novel potential engineered catalyst for catalytic degradation of orange II [J]. Journal of Cleaner Production, 2019, 221: 234 − 241. DOI: 10.1016/j.jclepro.2019.02.240.

[24] WANG Chong-qing, SUN Rui-rui, HUANG Rong. Highly dispersed iron-doped biochar derived from sawdust for Fenton-like degradation of toxic dyes [J]. Journal of Cleaner Production, 2021, 297: 126681. DOI: 10.1016/j.jclepro.2021.126681.

[25] RIBEIRO R S, SILVA A M T, FIGUEIREDO J L, et al. Catalytic wet peroxide oxidation: A route towards the application of hybrid magnetic carbon nanocomposites for the degradation of organic pollutants—A review [J]. Applied Catalysis B: Environmental, 2016, 187: 428 − 460. DOI: 10.1016/j.apcatb.2016.01.033.

[26] SHENG Yi-yi, SUN Yang, XU Jing, et al. Fenton-like degradation of rhodamine B over highly durable Cu-embedded alumina: Kinetics and mechanism [J]. AIChE Journal, 2018, 64(2): 538−549. DOI: 10.1002/aic.15937.

[27] ZHAO Su-xing, WANG Gai-rong, YANG Hong-ying, et al. Agglomeration-aggregation and leaching properties of mechanically activated chalcopyrite [J]. Transactions of

Nonferrous Metals Society of China, 2021, 31(5): 1465−1474. DOI: 10.1016/S1003-6326(21)65590-5.

[28] GRANATA G, TAKAHASHI K, KATO T, et al. Mechanochemical activation of chalcopyrite: Relationship between activation mechanism and leaching enhancement [J]. Minerals Engineering, 2019, 131: 280−285. DOI: 10.1016/j.mineng.2018.11.027.

[29] LIAO Rui, WANG Xing-xing, YANG Bao-jun, et al. Catalytic effect of silver-bearing solid waste on chalcopyrite bioleaching: A kinetic study [J]. Journal of Central South University, 2020, 27(5): 1395−1403. DOI: 10.1007/s11771-020-4375-1.

[30] ZANG Nan, WU Ze-xing, WANG Jie, et al. Rational design of Cu-Co thiospinel ternary sheet arrays for highly efficient electrocatalytic water splitting [J]. Journal of Materials Chemistry A, 2020, 8(4): 1799 − 1807. DOI: 10.1039/c9ta12104h.

[31] KHATAEE A, GHOLAMI P, VAHID B. Heterogeneous sono-Fenton-like process using nanostructured pyrite prepared by Ar glow discharge plasma for treatment of a textile dye [J]. Ultrasonics Sonochemistry, 2016, 29: 213−225. DOI: 10.1016/j.ultsonch.2015.09.012.

[32] ZHAO Qian-fei, YANG Hong-ying, TONG Lin-lin. Adsorption characteristics of CN−species on the chalcopyrite surface and its response to flotation [J]. Separation and Purification Technology, 2021, 276: 119322. DOI: 10.1016/j.seppur.2021.119322.

[33] HUANG Rong, YANG Jia-peng, CAO Yi-jun, et al. Peroxymonosulfate catalytic degradation of persistent organic pollutants by engineered catalyst of self-doped iron/carbon nanocomposite derived from waste toner powder [J]. Separation and Purification Technology, 2022, 291: 120963. DOI: 10.1016/j.seppur.2022.120963.

[34] YANG Jia-peng, HUANG Rong, WANG Lu-yao, et al. Efficient degradation of toxic mixed dyes through peroxymonosulfate activation by copper/iron nanoparticles loaded on 3D carbon: Synthesis, characterizations, and mechanism [J]. Journal of Environmental Chemical Engineering, 2022, 10(3): 107606. DOI: 10.1016/j.jece.2022.107606.

[35] WANG Chong-qing, HUANG Rong, SUN Rui-rui, et al. Microplastics separation and subsequent carbonization: Synthesis, characterization, and catalytic performance of iron/carbon nanocomposite [J]. Journal of Cleaner Production, 2022, 330: 129901. DOI: 10.1016/j.jclepro.2021.129901.

[36] WANG Huan-wei, FANG Xin, WAN Yu-chi, et al. Visible-light-induced $NiCo_2O_4$@Co_3O_4 core/shell heterojunction photocatalysts for efficient removal of organic dyes [J]. Journal of Central South University, 2021, 28(10): 3040−3049. DOI: 10.1007/s11771-021-4793-8.

[37] PENG Jia-li, ZHOU Hong-yu, LIU Wen, et al. Insights into heterogeneous catalytic activation of peroxymonosulfate by natural chalcopyrite: PH-dependent radical generation, degradation pathway and mechanism [J]. Chemical Engineering Journal, 2020, 397: 125387. DOI: 10.1016/j.cej.2020.125387.

[38] WU Li-yuan, GUO Peng-peng, WANG Xin, et al. The synergy of sulfur vacancies and heterostructure on CoS@FeS nanosheets for boosting the peroxymonosulfate activation [J]. Chemical Engineering Journal, 2022, 446: 136759. DOI: 10.1016/j.cej.2022.136759.

[39] FAN Bao-yan, LIU Hai-bo, WANG Zhen-hui, et al. Ferroelectric polarization-enhanced photocatalytic performance of heterostructured $BaTiO_3$@TiO_2 via interface engineering [J]. Journal of Central South University, 2021, 28(12): 3778−3789. DOI: 10.1007/s11771-021-4847-y.

(Edited by ZHENG Yu-tong)

中文导读

机械活化天然黄铜矿强化非均相Fenton催化降解废水中四环素

摘要：废水中有机污染物是环境领域亟待解决的难题之一，非均相高级氧化工艺是降解有机污染物的高效方法，然而，非均相高级氧化工艺受限于高效催化剂的开发。天然矿物具有廉价、资源丰富、环境友好等优点，用于非均相Fenton催化降解废水中有机污染物受到越来越多的关注。天然矿物的催化活性较低、如何提高天然矿物的催化活性是亟待解决的问题。本文提出机械活化提高天然黄铜矿的催化性能，通过非均相Fenton降解四环素评估催化活性变化。球磨10、30、60和120 min的天然黄铜矿对四环素的降解率分别为55.52%、68.97%、77.79%和86.43%，反应速率常数分别为0.0079、0.0109、0.0137和0.0192 min^{-1}，表明机械活化能显著提高天然黄铜矿的催化性能。通过表征分析发现，机械活化使黄铜矿的颗粒减小、比表面积增加、晶格尺寸减小、晶格畸变以及表面硫氧化。通过分析催化活性与黄铜矿不同参数的线性关系表明，催化活性提高主要归因于机械活化造成的比表面积增加与表面氧化。本研究表明机械活化能够提高天然矿物的催化活性，为开发天然矿物基高效非均相Fenton催化剂提供新的见解。

关键词：高级氧化工艺；黄铜矿；天然矿物；机械活化；四环素